On the role of Sc in powders and spray deposits of hypoeutectic Al-Mg alloys

S. Yin[1,2], A-A. Bogno[1], H. Henein[1], M. Gallerneault[2]

[1]Department of Chemical and Materials Engineering, University of Alberta
Edmonton, Alberta, Canada T6G 1H9

[2]Department of Mechanical and Materials Engineering, Queen's University, Kingston, Ontario, Canada K7L 3N6

Key words: Undercooling, atomization, powders, spray deposition, Al-Mg, scandium, solidification microstructures

Abstract

This paper studies the solidification of hypoeutectic Al-Mg-Sc powders and spray deposited (SD) strips, generated by Impulse Atomization, a type of drop tube. The effects of Mg content in hypoeutectic Al-Mg-Sc was examined with respect to the extended solid solubility of Mg and Sc in α-Al, microstructure refinement and heat treatment. Increasing Mg content from 1.5wt% to 3wt% yielded a reduction in dendrite cells spacing by 30% in the atomized powders, and up to 10% on SD samples, concomitantly with ~20% increase in hardness. Melt superheat appeared to yield a finer microstructure, as cell spacing of Al-3wt%Mg-0.2wt%Sc (T_L = 644°C) is found to be smaller than that of Al-1.5wt%Mg-0.2wt%Sc (T_L = 652°C), with both alloys atomized at the same temperature. The size of the primary structure in the powders was about five times larger than those of SD samples. The microhardness (Hv0.1) of powders and SD samples for the alloys is the same at ~45 and ~55 for the 1.5wt%Mg and 3wt%Mg alloys, respectively, despite the differences in primary structure of the solidified samples. Following a 2 hour aging time at 300°C, the hardness increases significantly (75-85 for 1.5wt%Mg samples and ~85 for 3wt%Mg samples). Thus, the scale of the primary structure in both powders and SD did not contribute to the differences in the hardness of the samples. It is apparent that

supersaturation during solidification is a determinant factor for the hardness of the alloys and is the same for both powders and SD for each respective alloy composition. Similarly, the precipitation of intermetallics and solid solution of the remaining solute after aging are the main contributors to the hardness increase in both alloy compositions. The aging effect of liquid droplets falling on an SD layer is similar to a new layer of melted powder solidifying over a former layer in additive manufacturing (AM). In SD, this leads to a supersaturation of the primary phase similar to that experienced in powders despite having a coarser primary structure. Similar effects are expected in AM samples. Thus, powders and SD samples are a good model for building a microstructure-property database in these class of alloys for other processes such as AM.

1. Introduction

Solidification structures of industrial alloys have an important effect on the mechanical properties of the alloys in service. The ability to control or vary the size of microstructure, the morphology of solidification products and the distribution of phases through the variation of alloy cooling rate or undercoolings can be undertaken in solidification processing. These parameters substantially affect the physical and chemical properties of metallic alloys. Rapid solidification (RS) results from high cooling rates and large nucleation undercoolings result in reduced microsegregation and often provide a broad range of metastable microstructures [1].

Minimizing the occurrence of solidification nucleation is one of the approaches to promote a high level of undercooling. Containerless solidification techniques are one approach to minimize nucleation induced by impurities from melt container walls [2]. Impulse Atomization (IA), a type of drop tube, is one of the most reliable containerless solidification techniques and has been used to analyze rapid solidification microstructures of a wide range of metallic alloys [3-11]. IA consists of generating liquid ligaments that break-up by Rayleigh instability into spherical droplets. These droplets fall and solidify by losing heat to a stagnant gas of choice (Ar, He, N_2, etc.). By breaking up the bulk liquid into fine droplets, IA provides containerless solidification advantages and isolates potential nucleation sites into small fractions of droplet populations. It has been shown in other studies [12-14] that a higher level of undercooling occurs as the atomized droplets solidify into powders or as a strip is deposited after landing in a semi-solid state on a substrate, termed Spray Deposition (SD) [3]. The oxygen concentration in the atomization chamber was minimized to <20ppm. But, the oxygen partial pressure (~70 mbar) is not low enough to prevent aluminum oxide formation on the droplets surface due to the high negative free energy of formation of aluminum oxide [15]. Consequently, a thin layer of aluminum oxide forms on the droplets surface as they fall. Thus, the semi solid droplets landing on a substrate are isolated from each other by the oxide layers. Hence, nucleation of subsequent phases (e.g. components of the eutectic) during further solidification occurs in each semi-solid droplet on the substrate independent of others surrounding it. Thus, eutectic or second phase particles nucleate in each of these deposited droplets

independently. This, results in additional primary phase forming under metastable conditions and will experience extended solid solubility and eutectic undercooling [16]. Thus, IA offers a unique means to achieve far-from-equilibrium microstructures through high cooling rates and large undercoolings for both powders and SD.

Aluminum alloys find many applications in the automobile and aerospace industries due to their high specific strength (density), excellent corrosion resistance and good formability. Transition metals (TM), such as Sc, are considered to form supersaturated solid solution during RS. Such supersaturation, which is the result of high undercooling, and controlled aging, can lead to substantial hardening and increased alloy strength. Under RS conditions such as those experienced in atomization, both TM and Mg can be present in Al alloys in solid solution. However, at Mg contents beyond ~3.5wt% can lead to stress corrosion cracking [17].

Small additions of Sc are reported to strengthen Al-Mg alloys [18]. The alloy must undergo age hardening. To reach good performance and to control the precipitation of Sc from a supersaturated solution, the alloy must be supersaturated in Sc [19]. In typical casting operations such as Direct Chill (DC) casting, low cooling rates (1°C/s to 10°C/s) are achieved [20]. For these typical casting operations, the supersaturation of Sc can only be obtained by homogenizing or solutionizing the alloy, followed by quenching. Due to the low solubility and diffusivity of Sc in aluminum, aging is carried out at high aluminum-processing temperatures (~500°C) for long times (~20 hours) [21].

In this work, IA was used to generate rapidly solidified Al-xMg-0.2wt%Sc (x=1.5, and 3wt%) powders and spray deposited strips (SD). Droplets produced by IA were collected as rapidly solidified powders during a run or were deposited onto a substrate before becoming fully solid (SD strip) during another run. Thus, by varying the droplet size, gaseous atmosphere and superheating [4, 5], tailored microstructures can be obtained. This paper studies the effects of IA, and SD induced rapid solidification on the resulting microstructures (cell spacing) and mechanical properties (hardness and yield strength) of

hypoeutectic Al-Mg-Sc. These two alloy compositions are selected due to their differences in solidification path as will be seen in the results section.

2. Materials and methods

2.1. Materials

IA was used to generate droplets of Al-xMg-0.2wt%Sc (x=1.5, and 3wt %). These samples were generated using various melt temperatures and atomized in an Ar or He atmosphere. The measured oxygen levels in the chamber were no greater than 10 ppm. A detail description of this process is given elsewhere [22]. In the current work, 350 grams of each investigated chemistry was pre-alloyed to the desired composition, heated to 200˚C above the alloy melting temperature and atomized. RS droplets traveled 4 meters below the atomization orifices and were solid when they were captured in oil at the bottom of the atomizing chamber. Strips were obtained using a spray deposition (SD) process [3]. The atomized droplets of median diameter (D50) around 350µm were in a mushy state (partially solidified) when they landed 0.4 m below the atomization orifices. The mushy droplets landed on a 3 mm thick copper substrate, moving at 0.038ms^{-1}. **Error! Reference source not found.** shows a schematic of the substrate and deposition assembly.

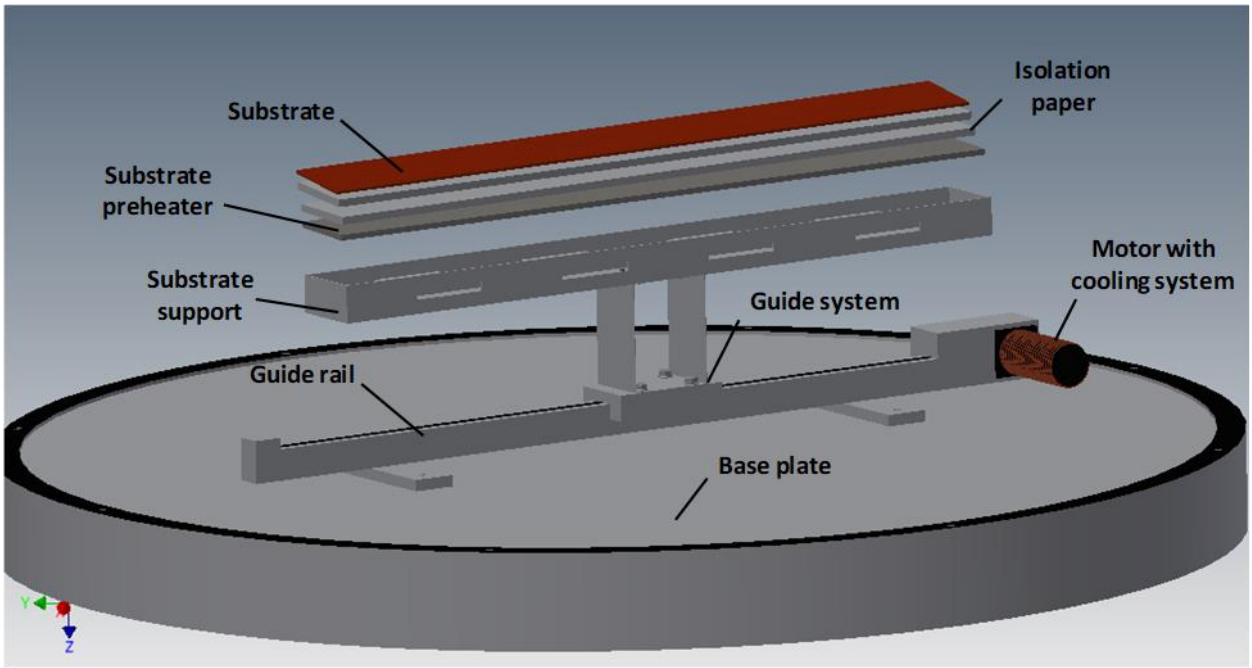

Figure 1: A schematic of the substrate movement system for Spray Deposition

The substrate is placed on a belt driven linear carriage/guide system, and is connected to a stepper motor (motor with cooling system). This ensures a controlled, reproducible substrate speed. The maximum displacement of the moving carriage was 650mm. A heating element is sandwiched between the substrate and the support. This heater provides heat to the substrate, thus removing any adsorbed water vapor. In the present work, prior to SD, the copper substrate was preheated to 100 ºC when the semi solid droplets spray landed upon it. A schematic description of the SD experimental setup is given in Figure 2.

Powders and strips with different thermal histories were generated for this study. Since Mg has a relatively high vapor pressure, the nominal concentration and the final concentration of Mg in the powders and SD strips may be different. Thus, the Mg content of the powders and SD samples were measured by inductively coupled plasma (ICP) spectrometry. The measured Mg concentrations of the atomized samples along with the experimental conditions are listed in Table 1.

The temperature history of the droplets cannot be measured in flight. Consequently, the cooling rate of any given droplet was determined by calculating it using a numerical model developed by Wiskel et al [4, 5].

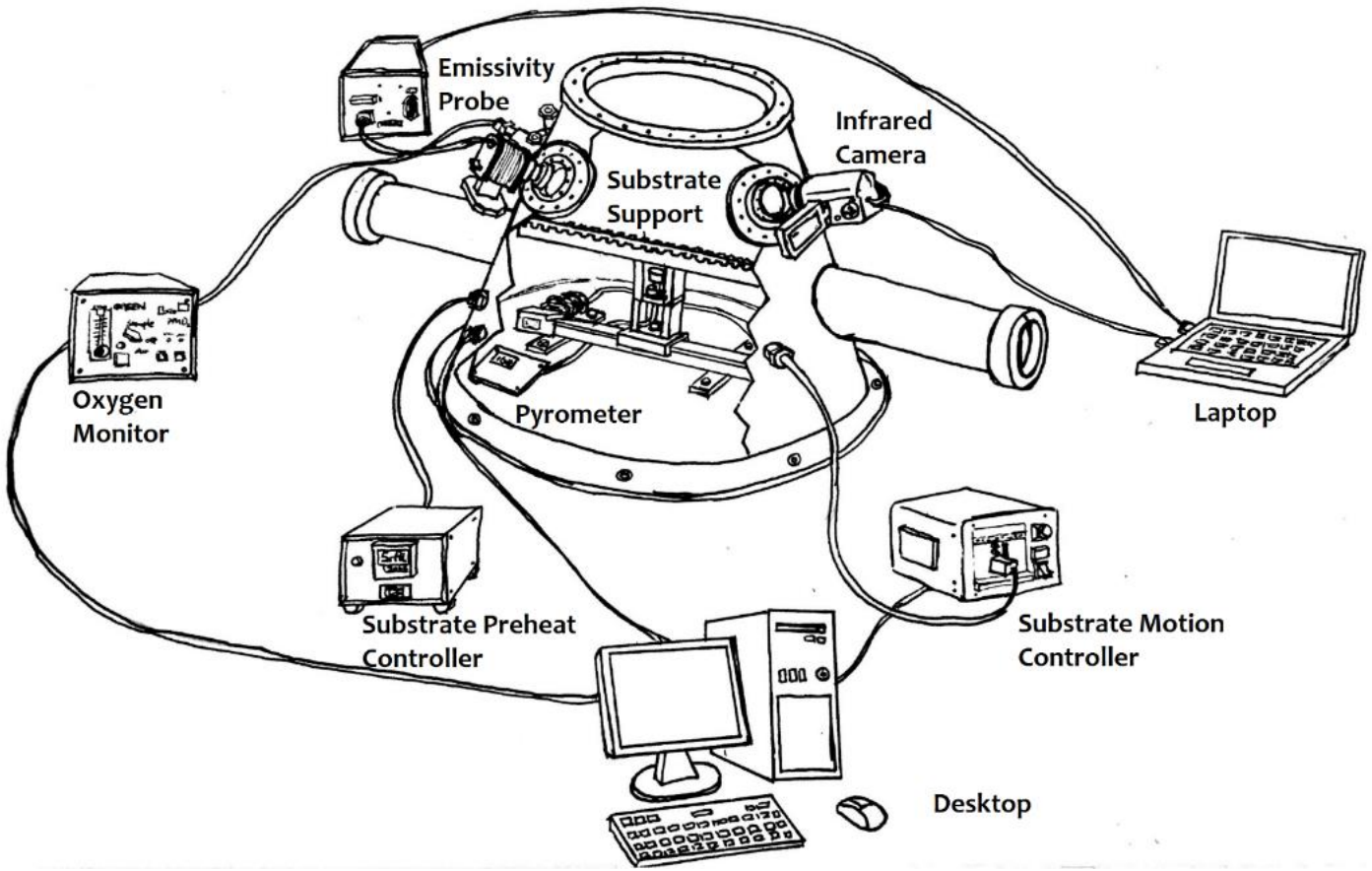

Figure 2: Schematic of the Spray Deposition (SD) set

Table 1. Summary of the investigated samples

Initial Composition [wt%]	Atomized Sample Mg [wt%]	T_{inital} [°C]	Shape
Al-1.53Mg-0.2Sc	1.46	900	Powder
	1.36	1000	SD Strip
	1.38	900	
	1.40	800	
Al-3.12Mg-0.2Sc	2.84	900	Powder
	2.78	1000	SD Strip
	2.91	900	
	2.98	800	

2.2. Microstructural Characterization

2.2.1. Microscopy

Scanning Electron Microscopy (SEM) was used to visualize the solidification microstructures and measure the microstructural length scale of the solidified samples. SEM analysis was carried out using a Tescan Vega3 equipped with an energy dispersive x-ray (EDX) analysis system (INCA Microanalysis System, Oxford Instruments). Imaging was done in backscattered electron (BSE) mode (to provide atomic number (Z) contrast), at an accelerating voltage of 10 kV. Prior to microscopy, the samples were mounted in epoxy resin, ground, and polished, (then etched with Keller's reagent for 10-20s for OM).

2.2.2. Cell spacing, hardness, and strength evaluation

The linear line intercept method (ASTM E112-13) was used on the 2D micrographs to measure the average secondary dendrite arms spacing, defined as the center-to-center distance between two dendritic cells. This microstructural length scale will be referred to as cell spacing in this paper.

The mechanical properties were evaluated through Vickers microhardness measurements of both the as-atomized (powders and strips), and heat-treated samples using a Buehler VH3100 microhardness tester, calibrated with a steel block (~62.5 Hv). A minimum of five indentations, with the indent size sufficiently large to measure across many dendritic cells were randomly applied to each sample with a load of 100 gf for a holding time of 10 s. The measured Vickers microhardness values (H_V) were subsequently converted to ultimate tensile strength (UTS) following the correlation given by equation 1, which was developed for ductile metals of young modulus E ≈ 70 GPA such as the alloy 6061 [23].

$$UTS = 3.07Hv - 4.32 \quad (1)$$

2.3. Aging treatment

Heat treatment procedure for Al alloys usually involves the dissolution of solute elements into the stable solid solution, α-Al phase (solutionising). To ensure that the solute is supersaturated in the primary α-Al, the sample is quenched into dry ice. This is followed by artificial aging at a specified temperature and for a desired time.

In this work, aging is carried out on the Al-Mg-Sc solidified samples directly without solutionizing, and quenching. Since the powder samples are rapidly solidified, it is expected that solute is supersaturated in the matrix. Consequently, there may be no need for solutionising so that samples can be directly aged after solidification. For the SD samples, it will be shown that the solute is also supersaturated in the α– Al primary phase. Hence, aging is achieved by heating the solidified samples to 300°C and holding for a desired amount of time before water quenching them to room temperature. Four different holding times were applied in this work: 0.5hr, 1hr, 1.5hrs and 2hrs. The aging process was carried out in an Hagaus Supermatic furnace .

2.4. High Temperature Heat Treatment

To demonstrate that the Al-Mg-Sc solidified samples were supersaturated with Sc, about 20mg of powders were used for the DSC analysis with a scanning rate of 0.3 °C/s from 30°C to a set temperature of 500°C. After reaching the set temperature, forced air was used

to cool the samples to room temperature. The Al-Mg-Sc samples were heated in a TA 2910 DSC using two alumina crucibles (sample and reference) and a Pt-Rh DSC rod. The DSC furnace was regulated by means of an S-type thermocouple (Pt/Pt-10% Rh) and was used to heat the samples in a protective nitrogen atmosphere.

The precipitation energy of Al_3Sc, and Al_3Mg_2 in an Al-Mg with minor Sc addition is considerably too small to be distinctly detected on the thermal profile. Therefore, pure aluminum was run in the DSC under similar conditions and the resulting curve was used as a baseline. The resulting temperature vs. energy curves of the alloy samples were subtracted from the pure aluminum baseline to identify precipitation events during heating.

3. Results and Discussions

3.1. Simulations and experimental observations of the solidification path

Figures 3a &3a' shows the solidification paths of both investigated alloys, as predicted by Gulliver–Scheil (GS) from the database TCAL8 in Thermo-Calc. Typical microstructure of the as-atomized samples of both investigated compositions are shown in Figure 3b & 3b'. The microstructures show primary dendritic α-Al (dark) surrounded by intermetallics rich grain boundaries (light). According to GS prediction, as can be seen in Table 2, Al-1.53wt%Mg-0.2wt%Sc microstructure consists (in mass fraction) of ~99% of primary α-Al and ~1% of Al_3Sc. Meanwhile, Al-3.12wt%Mg-0.2wt%Sc microstructure consists (in mass fraction) of ~97% primary α-Al, ~0.1% Al_3Sc and ~2.7% of eutectic α-Al +Al_3Mg_2.

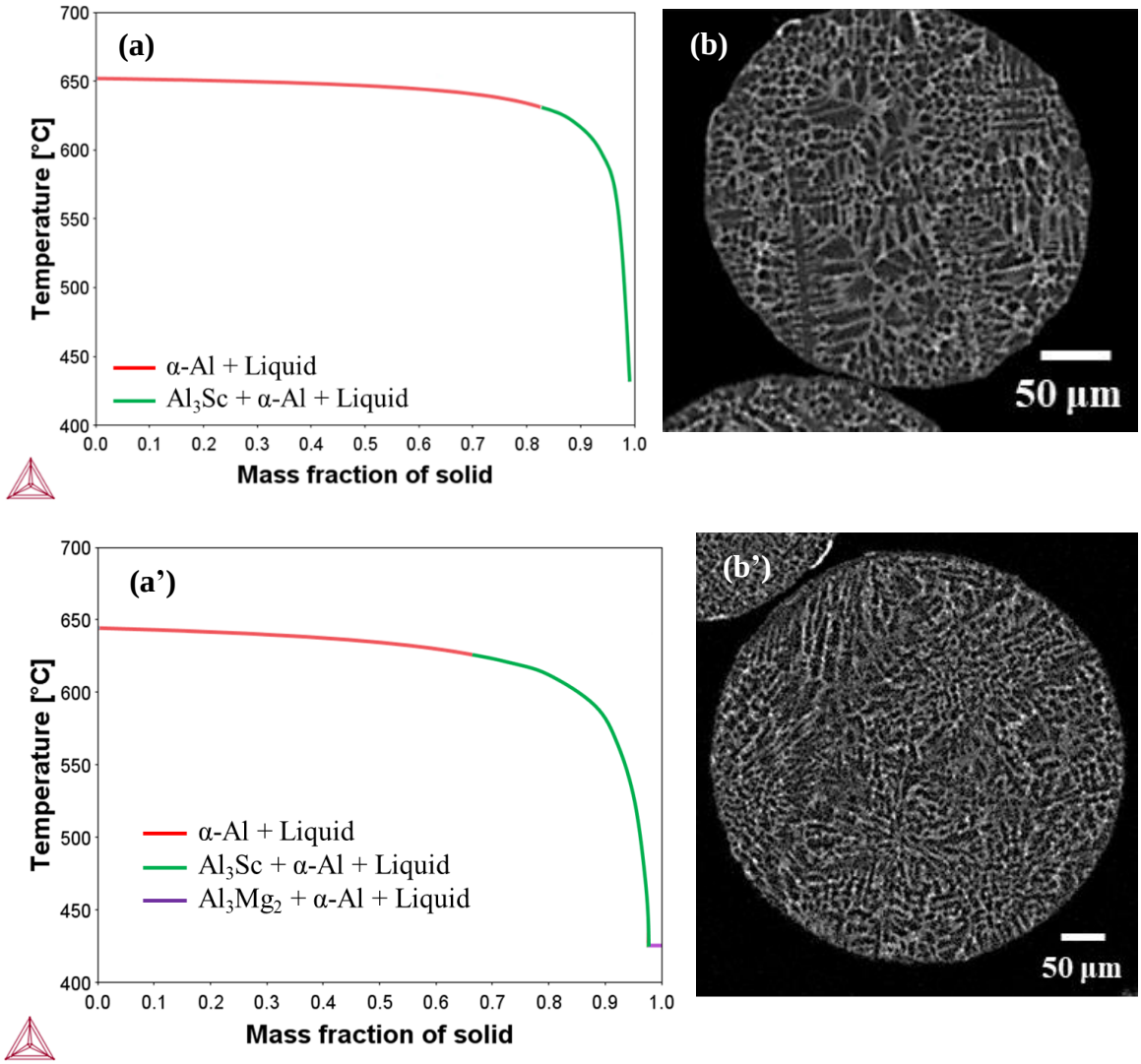

Figure 3: (*a-a') Gulliver-Scheil solidification path of Al-1.53wt%Mg-0.2wt%Sc and Al-3.12wt%Mg-0.2wt%Sc respectively, obtained through the database TCAL8 in Thermo-Calc©* [29], *and (b-b') Corresponding SEM micrograph of the alloys, from IA powders of 250µm - 300µm in size, showing primary dendritic α-Al (dark) surrounded by intermetallics rich grain boundaries (light).*

Table 2: Result of Gulliver-Scheil simulations (in Thermo-Calc© [29], *database TCAL8 for the two alloys, assuming the initial composition from Table 1*

Alloy composition, wt.%	Reaction equation	Temperature range, (°C)	Solid phase mass fractions at reaction end
Al-1.53Mg-0.2Sc	Liquid → (Al)	652-634	(Al): 0.824
	Liquid → (Al) + Al_3Sc	634-453	(Al): 0.990, Al_3Sc: 0.00958
Al-3.12Mg-0.2Sc	Liquid → (Al)	644 – 629	(Al): 0.603
	Liquid → (Al) + Al_3Sc	629 – 451	(Al): 0.972, Al_3Sc: 0.00082
	Liquid → (Al) + Al_3Sc + Al_3Mg_2	450, invariant	(Al): 0.976, Al_3Sc:0.00082, Al_3Mg_2: 0.0236

3.2. Cooling rates and microstructural length scales

Figure shows the relationship between the calculated cooling rate and the measured cell spacing for the powders produced. It is worth noting that, although dendritic arrangements are clearly observed in parts of the powder cross sections, the secondary dendrite arms are not clearly distinguishable in 2D. Therefore, the expression “dendrite cell spacing” or simply “cell spacing” is used for both the Secondary dendrite arms spacing and the spacing between the dendrite cross sections.

The cooling rates for powders in different size ranges are estimated by using the thermal model described in previous researches [4, 5].

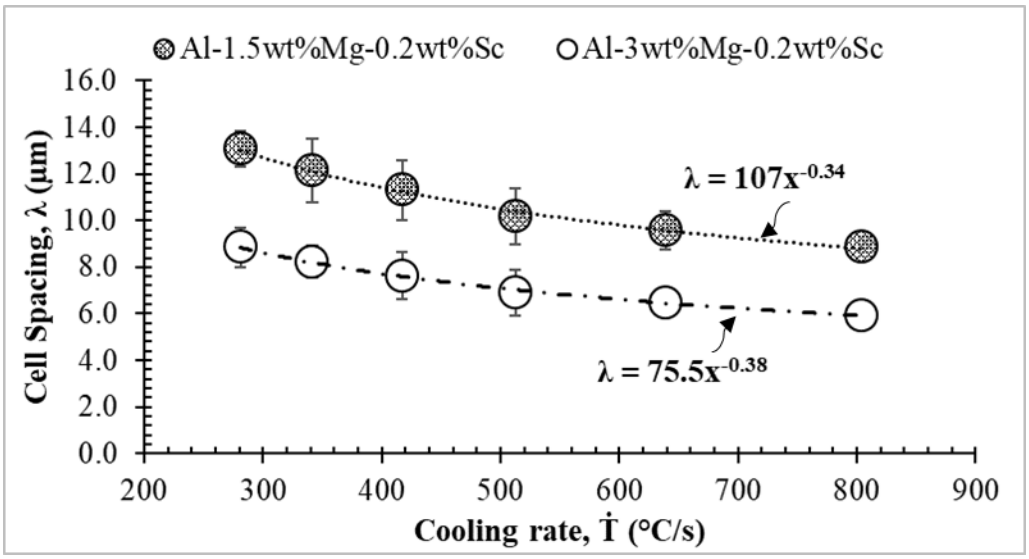

Figure 4: Variation of cell spacing with cooling rate of Al-xMg-0.2wt%Sc (x=1.5, and 3wt%) powders

Kurz and Fisher proposed a relationship between cooling rate and celling spacing [30]:

$$\lambda = B \cdot \dot{T}^{-n} \qquad 3$$

B is the empirical pre-exponential geometric factor B relating curvature differences to the cell spacing, and n is a constant. For both Al-1.5Mg-0.2Sc and Al-3Mg-0.2Sc *B* and *n* where estimated by curve fitting power functions to the experimental data.

Figure a shows cell spacing vs. location on the cross section of the SD strips. The cell spacing and cooling rate relationship established using powder samples were applied here to obtain the cooling rates for the SD strips based on the measured cell spacing. For each investigated alloy composition, there appears to be no variation of average cell spacing from top to bottom on the sample cross sections. The homogeneity of cell spacing might be a result of the high thermal conductivity of aluminum alloys and thin strip thickness.

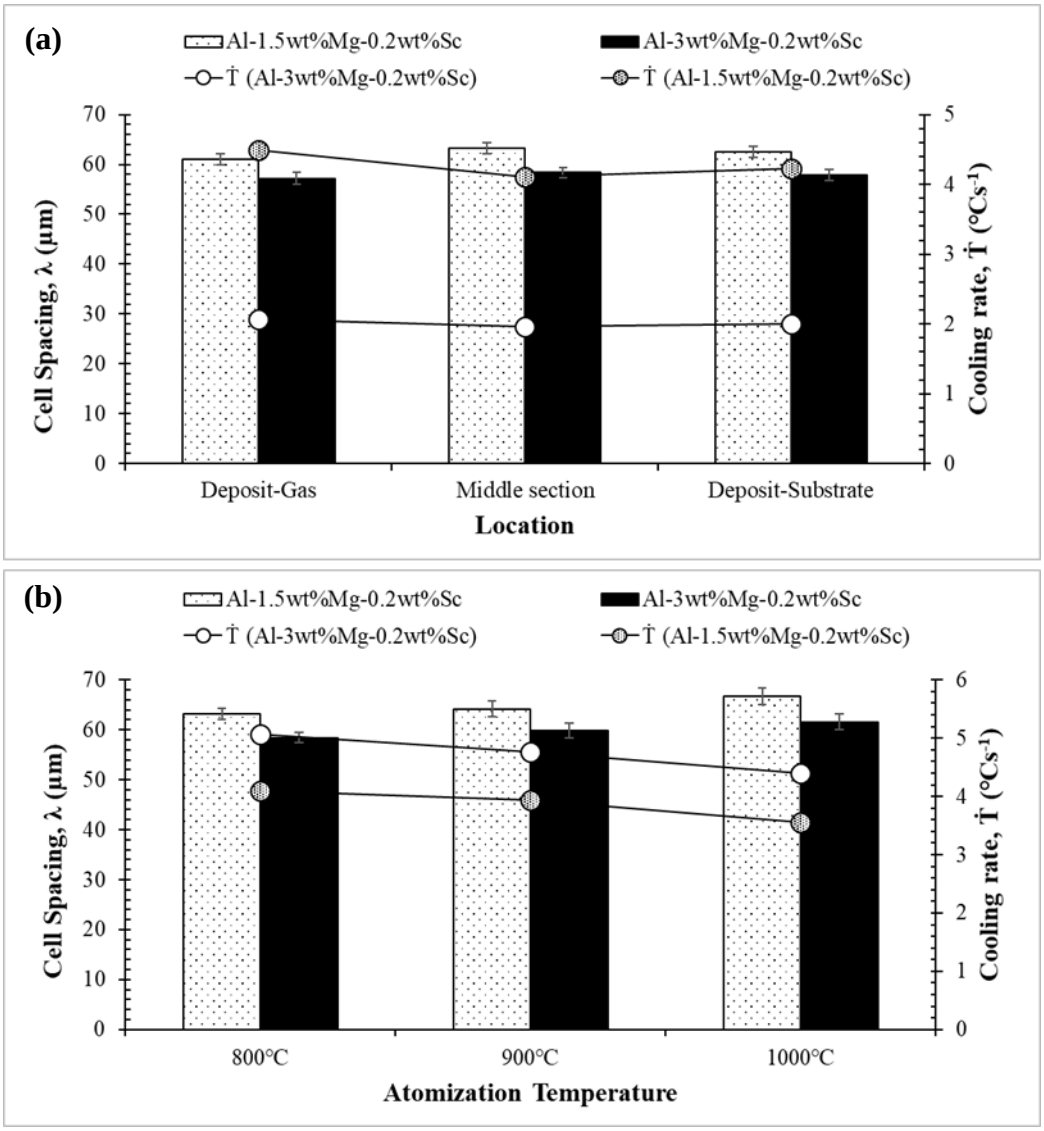

Figure 5: Variation of cell spacing and cooling rate within the cross section of SD Al-xMg-0.2wt%Sc (x=1.5wt% and x= 3wt %) strips as a function of (a) location on the strip cross section, (b) atomization temperature.

Figure b shows that the increase of atomization temperature does not lead to an increase in cell spacing. It is worth noting that the cell spacing in the strips are several times larger than those of powders (about 7 times the cell spacing of the largest investigated powder). This larger cell spacing, and therefore, cooling of the material, suggests that the melts fully solidified after landing on the copper substrate.

To compare the empirically determined pre-exponential geometric factor B in Equation 3, with a theoretical value using coarsening kinetics of the primary phase [30], and assuming n = 0.33, the following equations were used:

$$B = 5.5 \cdot (M \cdot \Delta T)^{0.33} \quad (4)$$

Where

$$M = \frac{\Gamma \cdot D \cdot ln\left[\frac{c_l^m}{c_o}\right]}{m \cdot (1-k) \cdot (c_o - c_l^m)} \quad (5)$$

M is the coarsening parameter, ΔT is the solidification interval, Γ is the Gibbs-Thompson coefficient; D is the diffusion coefficient of solute (Mg) in the liquid (Al), C_l^m is the composition of the last liquid to solidify (eutectic composition), C_0 is the alloy nominal composition (in this case, 1.5wt%Mg and 3wt%Mg), m is the slope of liquidus line, and k is the partition coefficient.

And

$$D = D_0 \exp\left(\frac{-Q_a}{RT}\right) \quad (6)$$

D is the diffusion coefficient (in m^2/s), D_0 is the maximal diffusion coefficient (at infinite temperature; in m^2/s), Q_a is the activation energy for diffusion (in J/mol), T is the absolute temperature (in K), and $R \approx 8.31446$ J/(mol·K) is the universal gas constant.

Property values for Al-1.53wt%Mg-0.2wt%Sc and Al-3.12wt%Mg-0.2wt%Sc are given in Table 3.

Table 3 Summary of Material Properties

Properties	Al1.5Mg	Al3Mg	Reference
D_0 (m^2/s)	$1.49 \cdot 10^{-5}$		[37]
Q_a (kJ/mol)	121		
Γ (K·m)	10^{-7}		[38]
c_l^m	15wt%	34wt%	[39]
c_o	1.5wt%	3.0wt%	
m	-0.16		
k	0.42		
ΔT	171	195	[29]
T_{start} (K)	925	918	
T_{end} (K)	754	723	

It is assumed that the 0.2wt% Sc has negligible effect on the coarsening of the primary phase. Also, assuming that the last liquid to solidify in Al-1.53wt%Mg-0.2wt%Sc alloy contains 15 wt% Mg (based on equations 4 to 6), the theoretical value of B is estimated to be in the range 26.9 to 105 depending on the diffusivity D, which varies throughout the solidification process. For the Al-3.12wt%Mg-0.2wt%Sc, the theoretical value of B ranges from 20.0 to 82.5. The empirically determined values given in Figure 4 are in relatively good agreement with the theoretically estimated values.

3.3. Mechanical properties of as-cast powders and strips

Figure 6a and Figure 6b show the Vickers microhardness measured respectively for the powders and the strips at different microstructural scales. Note that the hardness values of both alloys are in the same range for powders and SD strips despite the fact that the cell spacing is at least five times higher or more for the SD strips than for the powders.

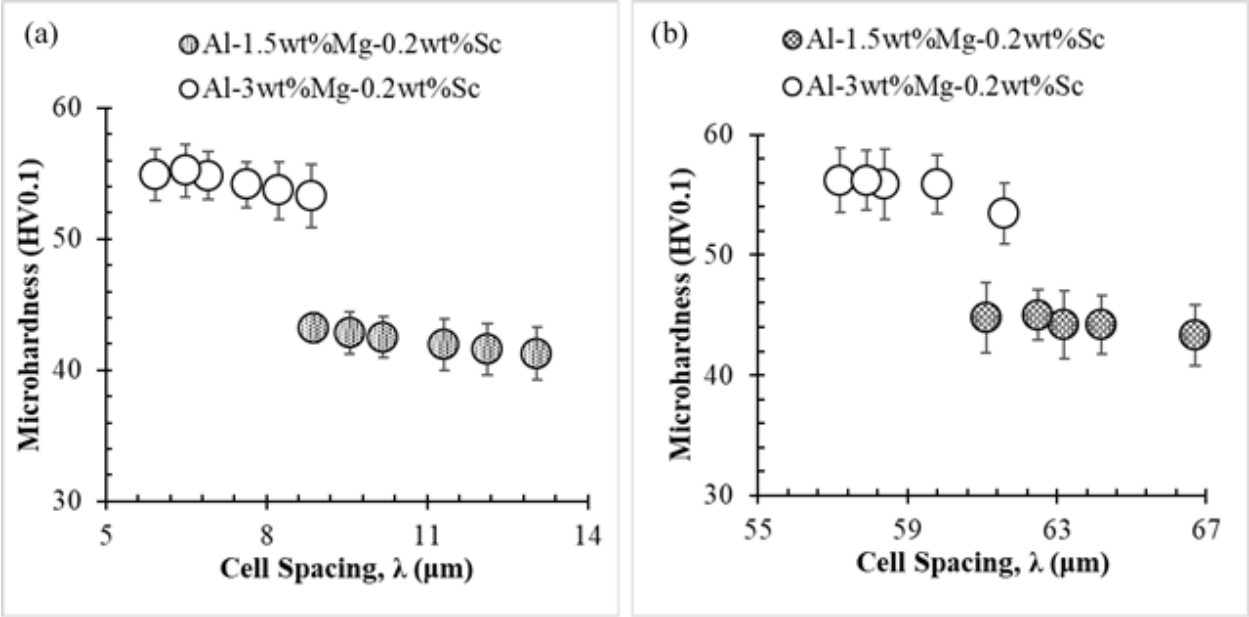

Figure 6: Variation of microhardness with cell spacing of as-cast Al-xMg-0.2wt%Sc (x=1.5wt% and x= 3wt%) (a) powders (b) SD strips

Al-3wt%Mg-0.2wt%Sc samples shows a higher microhardness than Al-1.5wt%Mg-0.2wt%Sc at similar size ranges. The extra hardening for Al-3wt%Mg-0.2wt%Sc is the result of the substitutional solid solution hardening effect of Mg. Due their similarity in size, Mg atoms substitute Al atoms in the α matrix lattice leading to a spherical strain field around the solute atoms due to the size and modulus differences between the Al matrix and the Mg solute atoms. The movement of dislocations will be blocked by this force field during deformation [31]. The hardness increase $\Delta\sigma_{ss}$ due to the addition of Mg could be estimated by using equation 7 below [32]:

$$\Delta\sigma_{ss} = H \cdot C^{\alpha} \qquad 7$$

Where C is the concentration of solute atoms, H and α are material constants that are found to be (in MPa/wt%) 13.8 and 1.14 respectively [33]. The $\Delta\sigma_{ss}$ difference between substitution in 3wt% Mg and 1.5wt% Mg is calculated to be 26.4 MPa. Recall that the hardness of the strip is the same as that of powders for the respective alloys, even though the cell spacing is dramatically different. Hence, the cell structure and size do not define the mechanical properties of the alloys. For the Al-Mg-Sc alloys, the mechanical properties

are defined by the level of substitutional solid solution of Mg in the Al matrix and the supersaturation of Sc (which is likely similar in both alloys).

3.4. Mechanical properties of aged powders and SD strips

One of the advantages of IA produced powders and deposits are the elimination of macro-segregation making the solute dispersed more homogeneous in the matrix than in a casting. Therefore, age hardening could be performed directly on the as-atomized samples without solutionizing, quenching then age hardening. In this study, the age hardening of the sample was carried out at 300°C and held for different aging times. The reason for age hardening at 300°C is that Al_3Sc precipitate, which is stated to promote the age hardening of Al-Mg alloys, is favored at this temperature [34].

Figure 7a shows the strength changes for powders at different age hardening times. Indeed, the Vickers microhardness numbers are converted to UTS as described earlier (section 2.2.2). For both alloys, the microhardness increases relatively rapidly in the first hour of aging treatment, then slightly slows down in the following half-hour, and flattened out afterwards. The age hardening plateau could be explained by the coherent particles, in this

case, the Al_3Sc precipitates, reaching their critical size r_{c2} which gives rise to the maximum strengthening effect [35].

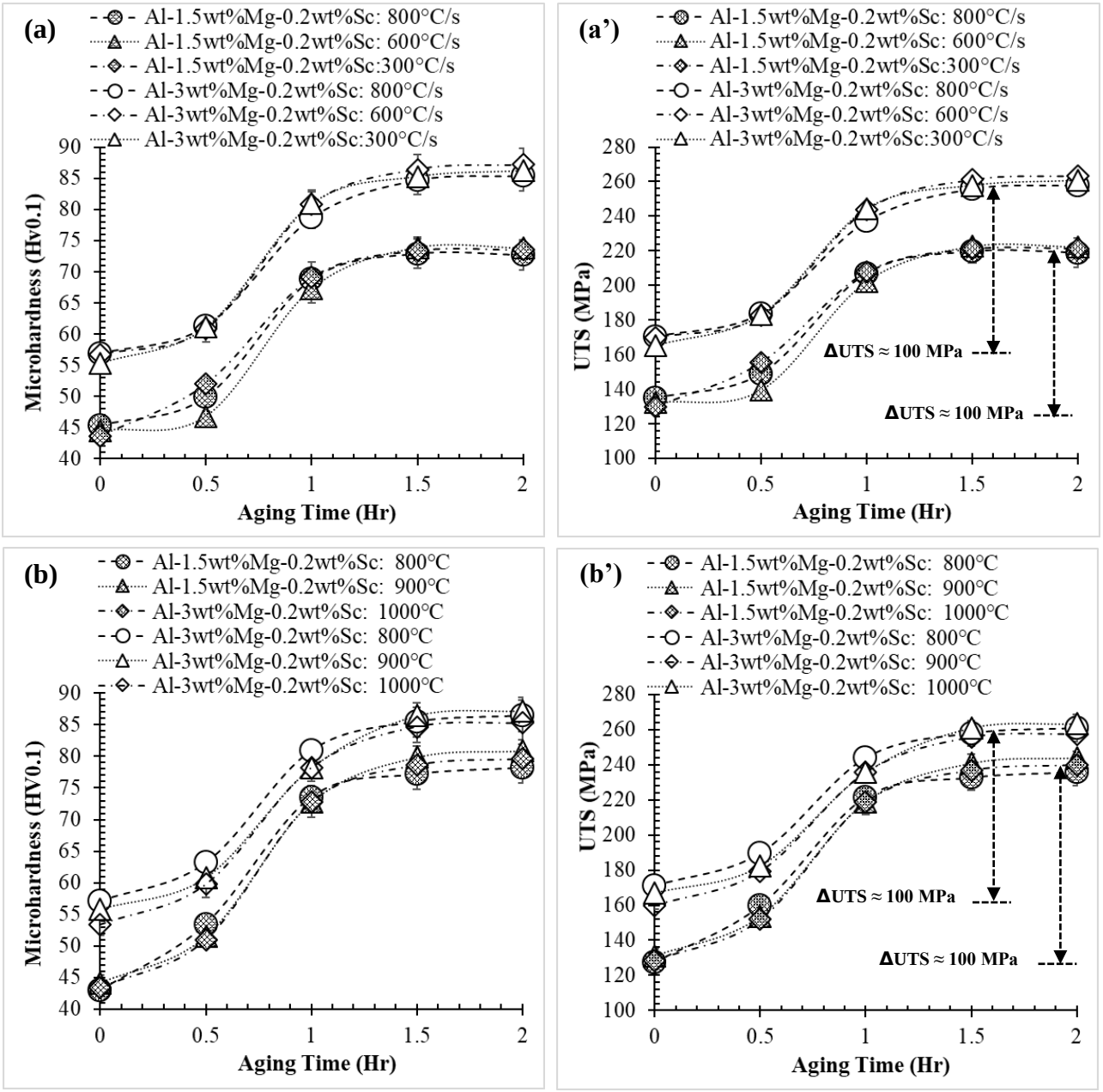

Figure 7: (a) Variation of microhardness and UTS of aged Al-xMg-0.2wt%Sc (x=1.5wt% and x= 3wt%) powders: (left) microhardness, (a', right) UTS. (b)Variation of microhardness and UTS at the deposit-substrate interface of Al-xMg-0.2wt%Sc (x=1.5wt% and x= 3wt%) SD strips generated from different atomization temperatures (left) microhardness and (b', right) UTS.

For powders with the same Mg level but different cooling rates, they started with a very similar microhardness. They followed a similar age hardening path, and finally reached nearly the same peak microhardness value. This similarity in the age hardening response suggests that the solute supersaturations is independent of powder solidification cooling rate.

For both Al-1.5wt%Mg-0.2wt%Sc and Al-3wt%Mg-0.2wt%Sc powders, at time zero, a difference in microhardness is observed due to the difference in Mg addition. After aging for 1.5 hours at 300°C, a similar microhardness difference is observed for both Al-1.5wt%Mg-0.2wt%Sc and Al-3wt%Mg-0.2wt%Sc. The additions of 1.5wt% Mg and 3.0wt% Mg do not seem to alter the age hardening effect of Sc. This could be explained by the extremely low solubility of Sc and Mg within each other [34] causing the availability of Sc for precipitates to remain unchanged despite the increased Mg level.

Figure 7b shows the age hardening evolution for SD strips produced at various atomization temperature. Similar age hardening responses were observed for the SD strips compared to the powders and about the same level of strength increase was achieved with the SD strips as with powders. It suggests that the Sc supersaturation is good enough to achieve a similar age hardening response. Despite the low cooling rate for the strips as shown in Figure (in the range of 2 to 5 °C/s), close to the those observed in traditional DC castings, the Sc supersaturation could still be achieved thanks to the same level of eutectic undercooling between powders and strips. With a relatively high undercooling, although the cooling rate is low, the reduced freezing range helps to shorten the cooling time required and therefore help to retain Sc in the matrix. This also underscores the value of the powders as a model system for SD deposits.

In all the cases, regardless of the cooling rate for powders or the atomization temperatures for the SD strips, the microhardness increased around 300MPa after aging, which represents a 60% increase of strength for Al-1.5wt%Mg-0.2wt%Sc and a 50% increase for Al-3wt%Mg-0.2wt%Sc materials. This shows the benefits of Sc addition to Al-Mg alloys. This is contrast to the work reported by Mochugovskiy and Mikhaylovskaya [36] where

Al-2.79wt.%Mg-0.15wt.%Zr and Al-2.79wt.%Mg-0.15wt.%Zr-0.1wt.%Sc alloys were solidified in a water-cooled copper mold. The HV of the as solidified alloys were around 50 HV similar to those of the powders and SD in this work. However, when aged hardened, the Zr containing samples achieved a maximum hardness of 65 to 66 HV. By contrast the RS powders and SD achieved a hardness of about 85 HV after heat treatment. Thus, RS has a more beneficial effect on the final strength of the alloy than the addition of Zr when processed using lower solidification conditions. Clearly RS enabled ultimately a finer and more homogeneous distribution of the L12-dispersoids after heat treatment due to its supersaturation during RS, resulting in a stronger alloy.

3.5. High temperature heat treatment

Al-Mg alloys with Mg concentration less than 5wt% do not have any response to age hardening and are non-heat-treatable. In this work, the increase in strength after aging is attributed to the addition of 0.2wt% Sc [31]. Differential scanning calorimetry (DSC) was done on powders and SD strip samples to see the how the heat flux changes (i.e. because of precipitation) as the samples are heated.

Figure 8a shows the temperature vs. heat flux plot in the DSC test results (two trials) for impulse atomized powders of Al1.5Mg0.2Sc in 600-710μm size range. A pure aluminum powder sample was first heated in the DSC with the same settings as for the alloy samples to be tested. A baseline for aluminum was then established. After the alloy samples were subsequently run in the DSC, the curve was then subtracted from the aluminum baseline curve to reveal any subtle heat flux changes. If no microstructural change occurs in the alloy, a smooth curve should be observed. In repeat runs, an exothermic heat flux can be observed starting at 285°C and ending at 365°C. This is indicative of some new phase forming, though in small volume fraction.

The isothermal sections of a corner of Al-Mg-Sc ternary phase diagrams at (b) 285°C, (c) 365°C are shown in Figure 8. At both temperatures, a mixture of Al and Al_3Sc phases should be expected. At 285°C, the higher driving force for the formation of Al_3Sc would lead to precipitation dominated process whereas at the 365°C and above, the reduced

driving force with the already established Al_3Sc precipitates during the heating up process would lead to a precipitate growth process, which would require a much lower thermal energy than the precipitation dominated process and therefore, the drop in heat flux could no longer be observed. Another possibility is that during the heating process, an equilibrium between Al and Al_3Sc is achieved at 365°C, i.e., the Al matrix is no longer saturated with Sc. This is less likely as the heating rate used was 20°C /min and the 4min between 365°C to 285°C should not be long enough for 0.2wt%Sc to precipitate out. Indeed, the Root Mean Square diffusion distance of Sc in Al at 300°C, was estimated to be only 192 nm for a holding time of up to 20 h [19]. Recall, the smaller cell spacings are for powders (Figure 8) and are at least one to two orders of magnitude larger than this diffusion distance.

Figure 8d shows the isothermal section of a corner of Al-Mg-Sc ternary phase diagram at 300°C. This is the age hardening temperature used in the current study. The low solubility of Sc in Al matrix would suggest a precipitation of Al_3Sc is preferred.

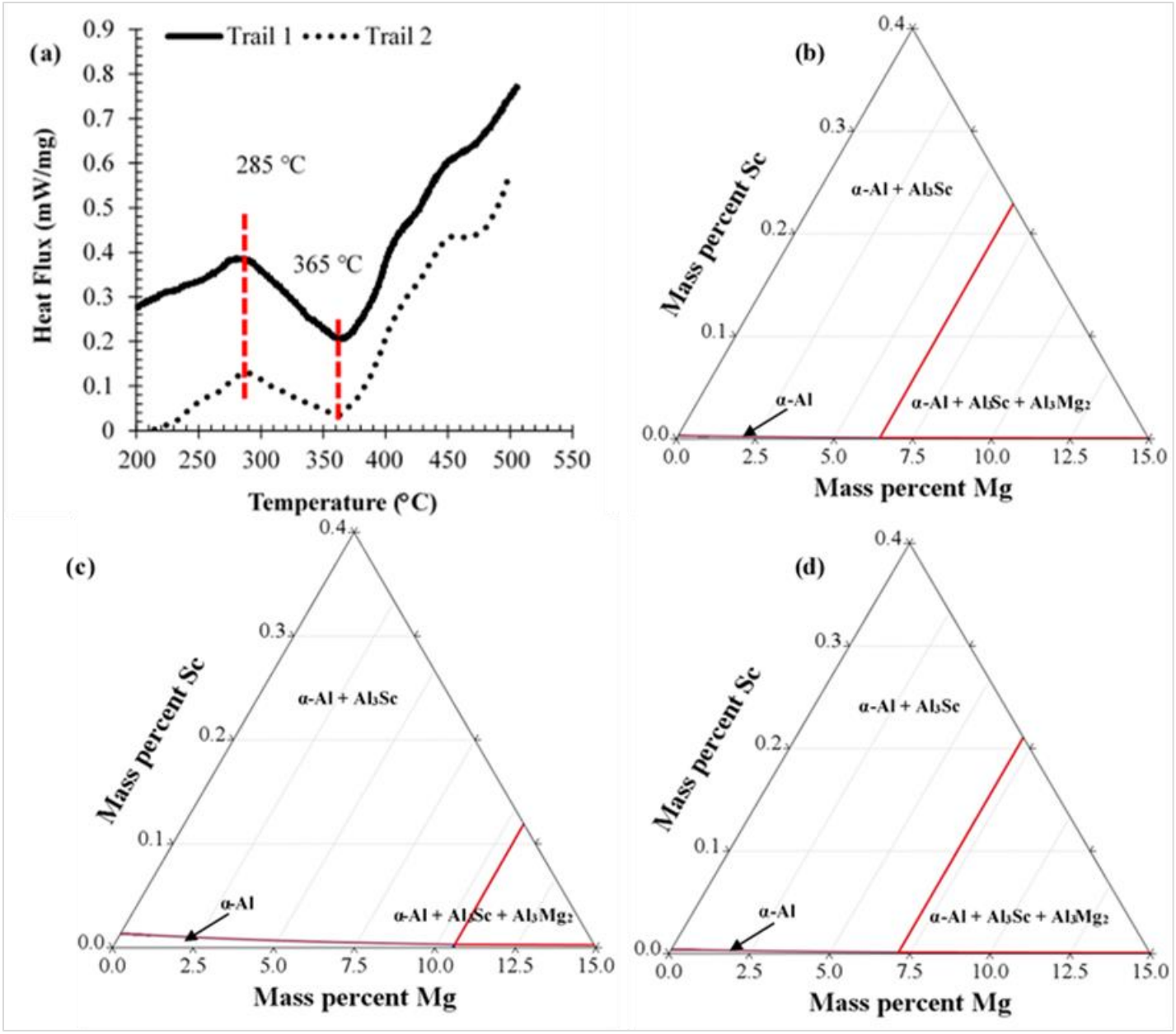

Figure 8: (a) DSC heat flux variation with temperature in two trials done on Al-1.5wt%Mg-0.2wt%Sc powders (600-710µm diameter), and an isothermal section of a corner of Al-Mg-Sc ternary phase diagram at (b) 285°C, (c) 365°C and (d) 300°C

4. Summary and Conclusions

Impulse Atomization (IA) successfully generated rapidly solidified Al-xMg-0.2wt%Sc (x=1.5, and 3wt%) powders and strips (by spray Deposition (SD)) in argon atmosphere. Our previous investigations demonstrated that rapid solidification enhances the solid solubility of Sc in aluminum, which lead to strong improvement of the mechanical properties upon aging. The Al-Mg-Sc system were studied and are a good model for commercial AA5xxx alloys. Two different Mg contents: Al-xMg-0.2wt%Sc (x=1.5, and 3wt%) were studied and reported here. The analyses resulted in the following conclusions:

- ✓ Microstructural scale does not have a noticeable effect on the microhardness of the powders and the strips. Thus, it is the solid solution of Mg that affects the microhardness and is not affected by Sc.
- ✓ Mg content does not contribute to the age hardening effect, it is rather the Sc addition that is responsible for the increase in hardness after aging through the formation of Al_3Sc precipitates from supersaturated Sc in the α-Al matrix.

Acknowledgements

The authors express their gratitude to to the Electron Microprobe Laboratory in the Department of Earth and Atmospheric Sciences, University of Alberta. The Natural Sciences and Engineering Research Council (NSERC) of Canada is gratefully acknowledged for their financial support and the support of the NSERC-HI-AM for partial support of one of the co-authors (A-A B) in the preparation of this manuscript.

References

[1] M. C. Flemings, Solidification Processing, London: McGraw-Hill, 1974.

[2] M. H. Dieter, and M. M. Douglas , Solidification of Containless Undercooled Melts, Germany: Wiley-VCH, 2012.

[3] N. Ellendt, R.-R. Schmidt, J. Knabe and H. Henein, "Spray Deposition using Impluse Atomization Technique," *Materials Science and Engineering:A,* vol. 1, no. 383, pp. 107-113, 2004.

[4] J. B. Wiskel, K. Navel, H. Henein and E. Maire, "Solidification study of aluminum alloys using Impulse Atomization: Part I: Heat Transfer Analysis of An Atomized Droplet," *Canadian Metallurgical Quarterly,* vol. 41, no. 2, pp. 97-110, 2002.

[5] J. B. Wiskel, K. Navel, H. Henein and E. Maire, "Solidifcation Study of Aluminum Alloys using Impulse Atomization: Part II. Effect of Cooling Rate on Microstructure," *Canadian Metallurgical Quarterly,* vol. 41, no. 2, pp. 193-204, 2002.

[6] H. Henein, "Single Fluid Atomization Through the Application of Impulse to a Melt," *Materials Science and Engineering A,* no. 326, pp. 92-100, 2002.

[7] J. Chen, U. Dahlborg, C. M. Bao, M. Calvo-Dahlborg and H. Henein, "Microstructure Evolution of Atomized Al-0.6wt%Fe and Al-1.90wt%Fe Alloys," *Metallurgical and Materials Transactions B,* vol. 42, no. 3, pp. 557-567, 2011.

[8] P. Delshad Khatibi, A. B. Phillion and H. Henein, "Microstructural Investigation of D2 Tool Steel during Rapid Solidification," *Powder Metallurgy,* vol. 57, no. 1, pp. 70-78, 2013.

[9] A. Ilbagi and H. Henein, "3D Quantitative Characterization of Rapidly Solidified Al-36wt%Ni," *Metallurgical Transactions A,* vol. 45, no. 4, pp. 2152-2160, 2014.

[10] N. Ciftci, N. Ellendt, R. Von Bargen, H. Henein, L. Mädler and V. Uhlenwinkel, "Atomization and Characterization of a Glass Forming Alloy," *Journal of Non-Crystalline Solids,* vol. 36, no. 42, pp. 394-395, 2014.

[11] A.-A. Bogno, J. E. Spinelli, C. R. Afonso and H. Henein, "Microstructural and Mechanical Properties Analysis of Extruded Sn-0.7Cu Solder Alloy," *Journal of Materials Research and Technology,* vol. 4, no. 1, pp. 84-92, 2015.

[12] I. T. Chang, B. Cantor and A. G. Cullis, "Metastable Ge-Sn Alloy Layers Prepared by Pulsed Laser Melting," *MRS Online Proceeding Library Archive,* vol. 407, p. 157, 1989.

[13] I. T. H. Chang, P. Svec, M. Gogebakan and B. Cantor, "Rapidly Solidified Al 85 Ni 15-x Y x (x=5,8,10) Alloys," *Materials Science Forum,* vol. 225–227, p. 335–340, 1996.

[14] C. R. Ho and B. Cantor, "Heterogeneous nucleation of solidification of Si in Al-Si and Al-Si-P alloys," *Acta Metallurgica et Materialia,* vol. 43, no. 8, pp. 3231-3246, 1995.

[15] D. Siemiaszko, B. Kowalska, P. Jóźwik and M. Kwiatkowska, "The Effect of Oxygen Partial Pressure on Microstructure and Properties of Fe40Al Alloy Sintered under Vacuum," *Materials (Basel),* vol. 8, no. 4, pp. 1513-1525, 2015.

[16] H. Henein, "Why is spray forming a rapid solidification process," *Materials Science and Engineering Technology, vol.41, no.7,* pp. 555-561, 2010.

[17] I. Polmear, Light Alloys -- Metallurgy of Light Metals 3rd ed., London: Arnold, 1995.

[18] V. L. Elagin, V. V. Zakharov and T. D. Rostove, "Scandium-alloyed aluminum alloys," *Metal Science and Heat Treatment,* vol. 34, no. 1, pp. 37-45, 1992.

[19] A.-A. Bogno, H. Henein, D. G. Ivey, J. Valloton, G. Reinhart, D. Sediako and M. Gallerneault, "Effects of Scandium on Rapid Solidified Hypo-eutetic Aluminum Copper," *Canadian Metallurgical Quarterly,* vol. 59, no. 1, pp. 101-115, 2020.

[20] M. Sohi, "Aging Behavior of Flexcast Al-Mg Alloys with Sc and Zr Additions," Master's dissertation ,The University of British Columbia, Vancouver, 2012.

[21] E. A. Marquis, D. N. Seidman and D. C. Dunand, "Effect of Mg addition on the creep and yield behavior of an Al-Sc alloy," *Act Materialia,* vol. 51, pp. 4751-4760, 2003.

[22] A. Prasad, "Microsegregation studies of rapidly solidified binary Al-Cu alloys," Ph.D thesis, University of Alberta, Edmonton, 2006.

[23] E. J. Arbtin and G. Murphy, "Correlation of Vickers hardness number, modulus of elasticity, and the yield strength for ductile metals," *Ames Laboratory ISC Technical Reports*, p. 50, 1953.

[24] W. Hearn, A.-A. Bogno, J. E. Spinelli, J. Valloton and H. Henein, "Microstructure Solidification Maps for Al-10wt%Si Alloys," *Metallurgical and Materials Transactions A* , vol. 50, no. 3, pp. 1333-1345, 2019.

[25] E. A. Brandes and G. B. Brooks, in *Smithells metals reference book*, London, Butterworths-Heinemann, 1998, pp. 14(1) - 14(4).

[26] A. A. Bogno, P. D. Khatibi, C. A. Gandin and H. Henein, "Quantification of dendritic and eutectic nucleation undercoolings in rapidly solidified hypoeutectic Al-Cu droplets," *Metall. Mater. Trans. A,* 47*, pp. 4606–4615,* 2016.

[27] S. Haferl and D. Poulikakos, "Transport and solidification phenomena in molten microdroplet pileup," *Journal of Applied Physics,* vol. 92, no. 3, pp. 1675-1689, 2002.

[28] A. A. Bogno, H. Henein and M. Gallerneault, "Design and Processing Conditions of Hypoeutectic Al-Cu-Sc Alloys for Maximum Benefit of Scandium," TMS 2018: *Light Metals 2018,* pp. 1609-1616, 2018.

[29] J. O. Andersson, T. Helander , L. Höglund, P. F. Shi and B. Sundman, *Thermo-Calc Software TTAL7 database,* 2002.

[30] W. Kurz and D. J. Fisher, in *Fundamentals of Solidification*, Trans Tech, 1989, pp. 85-87.

[31] M. Tiryakioglu and J. T. Staley, "Physical Metallurgy and the Effect of Alloying Additions in Aluminum Alloys," in *Handbook of Aluminum, Volume 1 Physical Metallurgy and Processes*, New York, Marcel Dekker, Inc, 2003, pp. 81-210.

[32] T. Suzuki, S. Takeuchi and H. Yoshinaga, " *Dislocation Motion in the Field of a Random Distribution of Point Obstacles: Solution Hardening. In: Dislocation*

Dynamics and Plasticity", Springer Series in Materials Science, vol 12. Springer, Berlin, Heidelberg, pp. 32-46, 1991.

[33] D. J. Lloyd and S. A. Court, "Influence of grain size on tensile preperties of Al-Mg allous," *Materials Science and Technology,* vol. 19, no. 10, pp. 1349-1354, 2003.

[34] M. S. Kaiser, S. Datta, A. Roychowdhury and M. K. Banerjee, "Age hardening Behavior of Wrought Al-Mg-Sc Alloy," *Materials and Manufatcturing Processes,* vol. 23, no. 1, pp. 74-81, 2007.

[35] Z. Guo and W. Sha, "Quantification of Precipitation Hardening and Evolution of Precipitates," *Materials Transactions,* vol. 43, no. 6, pp. 1273-1282, 2002.

[36] A. G. Mochugovskiy and A. V. Mikhaylovskaya, "Comparison of precipitation kinetics and mechanical properties in Zr and Sc-bearing aluminum-based alloys," *Materials Letter*, vol. 275, pp. 1-4, 2020.

[37] Y. Du, "Diffusion coefficients of some solutes in fcc and liquid Al: Critical evaluation and correlation," *Material Science and Engineering,* vol. A, no. 363, pp. 140-151, 2003.

[38] D. Stefanescu, "Equilibrium and non-equilibrium during soldification," in *Science and Engineering of Casting Soldification, 2nd Edition*, Columbus, Springer, 2002, pp. 5-24.

[39] H. Baker, "Alloy Phase Diagrams," in *ASM Handbook,* ASM International, 1992, p. Vol 3.

[40] M. Tiryakioğlu and et al, "Hardness–strength relationships in the aluminum alloy 7010 Materials," *Science&Engineering*, vol. A631, pp. 196-200, 2015.

[41] E. J. Pavlina and C. J. Van Tyne, "Correlation of Yield Strength and Tensile Strength with Hardness for Steels," *Journal of Materials Engineering and Performance,* vol. 17, no. 6, pp. 888-89, 2008.